A 32-Gigahertz Traveling-Wave Maser Design

J. Shell[1] and R. Clauss[2]

A new 32-GHz traveling-wave maser design is presented. The new ruby maser design uses a very simple slow-wave structure consisting of a smooth rectangular waveguide with no metal irises or steps. Ruby-filled and evanescent sections of waveguide form resonators, creating a slow-wave structure with high slowing factors at both the signal and pump frequency bands. This approach results in a high gain–bandwidth product at the signal frequency and efficient use of pump power, thereby reducing the heat load. Advantages of this approach include reduced machining costs and the ability to operate the maser in a commercially available 4-K Gifford–McMahon cycle refrigerator.

I. Introduction

This article describes the design, the analysis tools, and the performance analysis for a new maser. The design uses coupled ruby resonators configured as a traveling-wave maser (TWM) at the Ka-band deep-space-to-Earth allocation of 31.8 GHz to 32.3 GHz. The maser may operate with an instantaneous bandwidth between several hundred to 500 MHz depending on the biasing magnetic field shape used. With the narrow bandwidth option, it is tunable over the Ka-band frequency allocation. The maser is planned for operation in a closed-cycle helium refrigerator at a physical temperature of 4 K or below. Advantages of the new design include (1) a slow-wave structure that is simple to machine, with no metal discontinuities (steps or irises) in the amplifying region, and (2) low loss and low group velocity at both the signal and pump frequencies, thereby maximizing the gain and bandwidth at Ka-band while minimizing the required pump power at V-band (65.75 GHz to 66.75 GHz).

Ruby masers are very robust. They are not susceptible to microscopic failure or burnout due to watt-level input signals or bias/supply-voltage transients. They are not sensitive to out-of-band radio frequency interference, are very linear, and do not produce measurable intermodulation products. This maser design should have a lower noise temperature than the best high-electron mobility transistor (HEMT)-based amplifiers available today. Performance is improved if the maser is cooled below 4 K.

II. Background

Recent years have seen the development of a coupled-cavity maser design [1]. That design was tunable over the full 500-MHz frequency allocation from 31.8 to 32.3 GHz, but the instantaneous bandwidth would

be near 100 MHZ, much less than 500 MHz. Broadening the paramagnetic spin resonance line width over a very small piece of ruby in order to achieve wide bandwidth is also a challenging task. If more than one ruby is used, the static (biasing) magnetic field staggering is simplified, and a wider instantaneous bandwidth can be achieved. Originally, multiple-ruby reflection-type amplifiers were considered. However, computer modeling and analysis indicated that mechanical construction tolerances would be difficult to meet. A traveling-wave maser design was developed, analyzed, and determined to have less stringent tolerances than the reflection-type amplifier.

The process of analyzing the reflection-type designs led to the realization that a simple uniform metal waveguide slow-wave structure could be used. Changes in wave impedance are created by changes in the dielectric constant of the material filling the waveguide channel. These changes in dielectric constant provide the necessary discontinuities to form the slow-wave structure. This design offers the best maser performance in a simple way, leading to the lowest cost.

The production and commercial availability of Gifford–McMahon (GM) cycle two-stage coolers with 1.5-W capacity at 4.2 K greatly simplify the use of masers. Previous operational DSN maser systems depended upon the use of JPL-designed and -built 4.5-K cryogenic systems [2,3]. A system of Joule–Thomson (J-T) counter-flow heat exchangers and a J-T valve are used to produce liquid helium in a closed-cycle system. This J-T loop is pre-cooled by a two-stage GM cooler to reduce the helium gas temperature far below the inversion point, a fundamental requirement of the Joule–Thomson cooling process. These DSN systems initially had a 1-W cooling capability at 4.5 K and were later improved to achieve a 2-W cooling capability at 4.5 K. A small number of masers in the DSN were cooled in open-cycle helium dewars, some at 4.2 K, and more recently two experimental units were cooled in super-fluid helium at 1.5 K [4,5].

Operating masers at temperatures below 4 K improves performance but requires the maser to operate in a refrigerator where the final stage has limited cooling capacity. The reduced-temperature-operation possibility provided a strong incentive to develop a new maser that would operate with low pump-power levels. Our goal for the pump-power heat load on the final stage was to be less than 100 mW, preferably less than 50 mW.

Following a brief description in Section III of the computer programs useful in designing the maser, the key features of the microwave structure are presented. This article does not discuss the superconducting magnet design or further aspects of cooling the maser. The discussion is limited to the microwave structure. A perspective view of the maser is shown in Fig. 1(a). A top view is shown schematically (not to scale) in Fig. 1(b). The slow-wave structure (SWS), between planes c–d and c′–d′, is discussed in Section IV. The microwave circuit used to transform between the WR-28 waveguide and the SWS, between planes a–c and a′–c′, is discussed in Section V. The U-turn cavity, between planes d–d′ and e–e′, is discussed in Section VI. The microwave circuit used to inject the pump power into the U-turn cavity, between planes e–e′ and f, is discussed in Section VII. Broadening of the ruby paramagnetic resonance line width with a linearly tapered biasing dc magnetic field is discussed in Section VIII. A discussion of the distributed resonant ferrite isolator used to provide reverse loss is discussed in Section IX. Section X discusses the estimated noise performance and measurements that are planned before the maser is built.

The maser is built completely using rectangular waveguide; no coaxial components are used. The maser is U-shaped for several reasons. The U-turn cavity provides a convenient point to inject the pump energy into the two arms of the SWS. Second, it reduces the overall length of the maser, thus reducing the size of the biasing magnet. Third, with a linear magnetic field taper along the SWS, a more uniform noise temperature distribution with frequency is achieved. Finally, the spin resonant frequencies of the ruby resonators in the two arms can be offset so as to compensate for the regions in the SWS where there is no ruby.
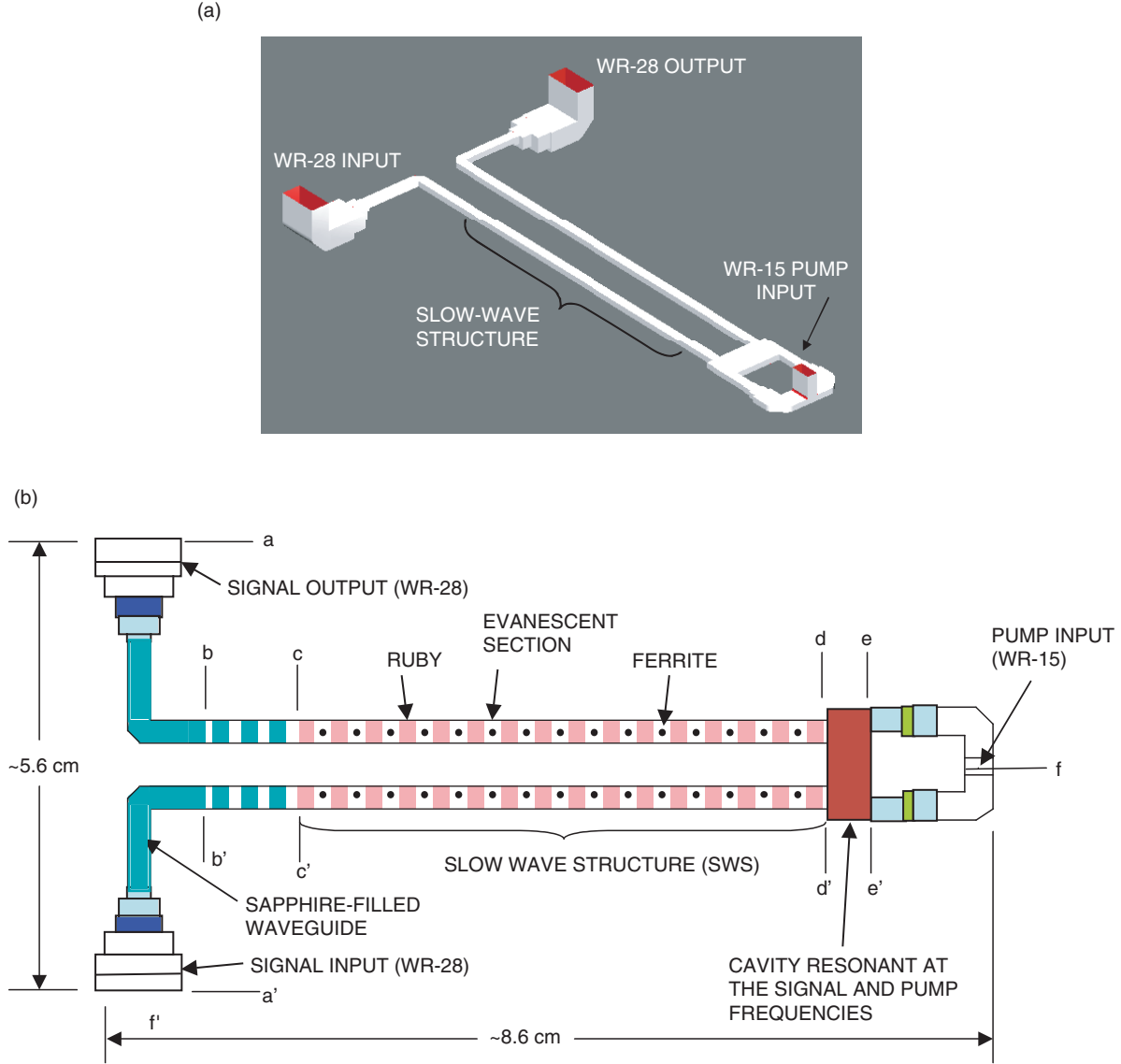
(a)

WR-28 OUTPUT

WR-28 INPUT

WR-15 PUMP INPUT

SLOW-WAVE STRUCTURE

(b)

a

SIGNAL OUTPUT (WR-28)

EVANESCENT SECTION

RUBY

FERRITE

b   c

d   e

PUMP INPUT (WR-15)

~5.6 cm

b'

c'

SLOW WAVE STRUCTURE (SWS)

d'   e'

f

SAPPHIRE-FILLED WAVEGUIDE

SIGNAL INPUT (WR-28)

a'

CAVITY RESONANT AT THE SIGNAL AND PUMP FREQUENCIES

f'

~8.6 cm

Fig. 1. The maser microwave structure: (a) perspective view and (b) schematic view (not to scale).

III. Computer Programs Useful in the Design Process

Two Fortran 90 computer programs were developed previously to aid in maser design. One of these programs calculated the microwave magnetic field in a coupled-cavity system [6]. The second program used this information to reduce the ruby magnetic susceptibility tensor to a scalar [7]. A conventional mode-matching algorithm calculated the scattering parameters. In order to speed the design process, these two programs were combined into one program. In addition, a few improvements were made. First, the allowed number of ruby resonators was increased from one to a user-specified number. Second, a biasing magnetic field variation in any direction was allowed. Previously, a variation only along the direction of signal propagation was allowed.

The combined program can be run in one of three modes, depending on the user's needs. In the first mode, it calculates scattering parameters of microwave structures without a paramagnetic spin system present. This calculation follows that described by Hoppe [8]. In the second mode, the microwave

electric and magnetic fields are calculated at a particular frequency in certain user-specified regions of the microwave structure. In this mode, the scattering parameters are not calculated and again no spin system is present. This mode is primarily used as an aid in understanding the electromagnetic behavior of the structure.

In the third mode, the microwave magnetic field is calculated at a chosen frequency in the regions containing the ruby spin system. Along with the assumed resonance frequency spatial distribution, a position-dependent effective complex scalar susceptibility is calculated. This scalar susceptibility modifies the complex permeability used in the original mode-matching program. Then the scattering parameters, including the ruby gain or absorption, for the complete microwave structure are calculated.

The waveguide width, the ruby length, and the spacing between the rubies are selected with the help of equations found in the appendix. The quarter-wave transformers used to impedance match the SWS to a sapphire-filled waveguide are also designed based on equations found in the appendix. These equations were implemented in simple programs to speed the design process. A MATLAB [9] program solves the spin Hamiltonian for ruby. This determines the biasing magnetic field strength, and the frequencies, transition probabilities, and spin vectors for transitions between the quantum levels of interest [10]. Finally, a program was used to generate the input files for the mode-matching program. In particular, the resonance frequency distribution for the 32 rubies was calculated once the start and stop frequencies were specified.

In addition to the programs written by the authors, a commercially available computer program was used in this project [11]. Initially, the program verified the behavior of the U-turn cavity. (The maser mode-matching program modeled this U-turn as an S-bend.) Later it was used to analyze the E-plane T-junction and the H-plane mitre bend used in the pump circuit. It also was used to analyze the E-plane mitre bend in the WR-28 waveguide and the H-plane mitre bend in the sapphire-filled waveguide (between planes a and b of Fig. 1). It is a very versatile program, but cannot model the paramagnetic spin system response at the signal and pump frequencies.

IV. Slow-Wave Structure

The function of the SWS is to increase the interaction time between the signal and the ruby spin system. The rubies act as resonators, and sections of evanescent waveguide provide the coupling between resonators. Although the fields decay exponentially in the evanescent sections, these sections should still be considered as part of the "resonator."

A fast and simple method of calculating the multiple pass bands and stop bands of a potential SWS consisting of propagating and evanescent sections of waveguide is useful. The maser designer can vary the waveguide width and relative dielectric constants and quickly determine if a suitable choice has been made. Our method is based on the use of wave transmission matrices [12]. Consider the slow-wave structure shown in Fig. 2. A "unit cell" can be defined between terminal planes 1 and 4. The slow-wave structure consists of this unit cell translated in the direction of propagation. The wave amplitude transmission matrix for the unit cell can be constructed by multiplying 5 transmission matrices. The first matrix describes propagation in the ruby between planes 1 and 2. The second matrix describes the ruby–air interface at plane 2. The third matrix describes propagation between planes 2 and 3, the evanescent section of waveguide. The fourth matrix describes the air–ruby interface at plane 3. The fifth matrix describes propagation in the ruby between planes 3 and 4. The reader is referred to the appendix for the details of the wave amplitude transmission matrices and the formula for the propagation constant. A pass band occurs at those frequencies for which the propagation constant is imaginary, and a stop band at those frequencies for which the propagation constant is real.

The SWS design uses nearly square ruby resonators. The width and length are 0.174 cm (0.0685 in.) and 0.1715 cm (0.0675 in.), respectively. We have assigned a relative dielectric constant of 10.1 to the
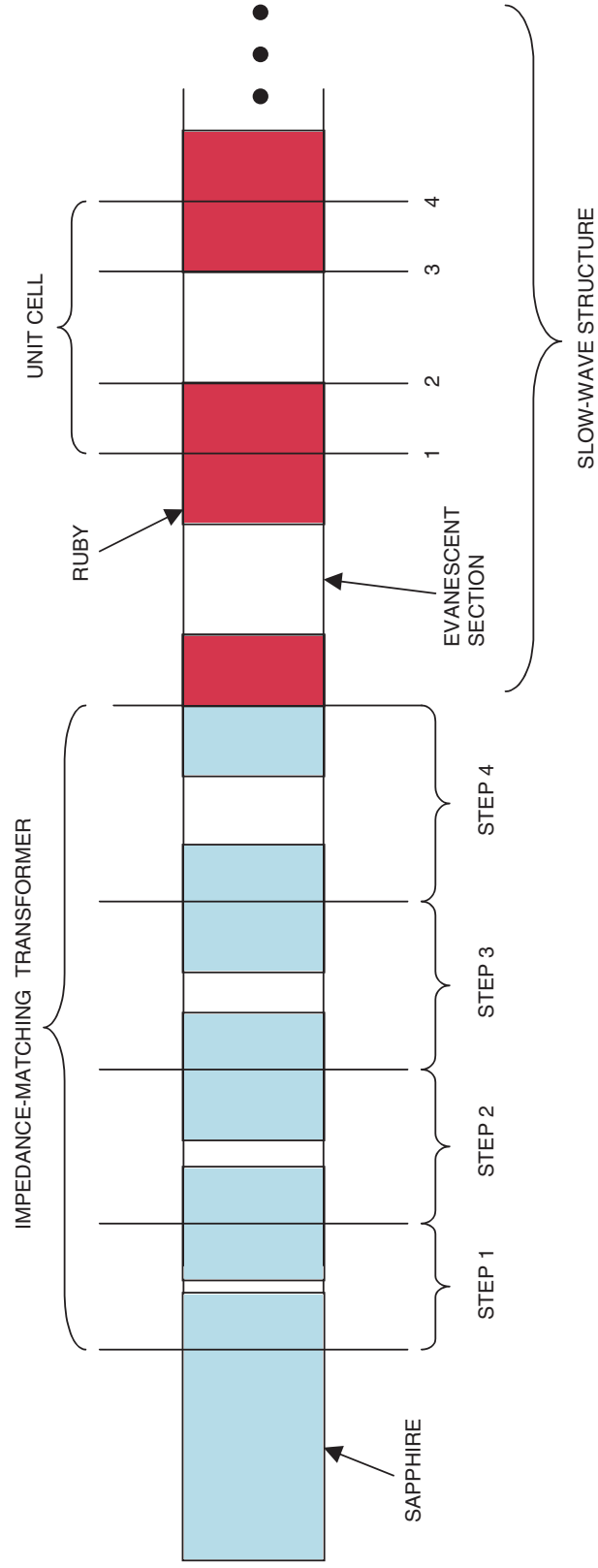
Fig. 2. The slow-wave structure unit cell and impedance-matching transformer.

ruby. The width and length of the evanescent sections are 0.174 cm (0.0685 in.) and 0.127 cm (0.050 in.), respectively. The three lowest pass bands are shown in Fig. 3. Frequency is plotted on the vertical axis, and the radian phase shift through a unit cell normalized by π is on the horizontal axis. One pass band is centered around 32 GHz, the second is centered around 46 GHz, and the third is centered around 66 GHz.

With appropriate impedance-matching sections, the transmission behavior of the SWS at 32 GHz is shown in Fig. 4(a). At this frequency, the rubies and evanescent sections form half-wavelength resonators. Correspondingly, with appropriate matching sections, the transmission behavior of the SWS at 66 GHz is shown in Fig. 4(b). At this frequency, the rubies and evanescent sections form 1.5 wavelength resonators. Good transmission centered around 66.25 GHz is necessary to effectively pump all the rubies. Slowing at the pump frequency increases the interaction time with the pump energy. This is particularly advantageous since the quantum mechanical transition probability for exciting spins at the pump frequency is weak. A plot of the group delay of one arm of the SWS at the signal frequencies is shown in Fig. 5. The bandwidth of the SWS has been chosen so the variation in group delay from 31.8 to 32.3 GHz is not excessive. Otherwise a significant gain variation would result when the ruby is amplifying. The total group delay through both arms of the SWS is about 10 ns. This compares with approximately 16 ns for the wide-bandwidth Ka-band reflected wave maser built in 1988 [13]. The reflected wave maser used 8 bars of ruby. Each bar was about 7.6 cm long. The total volume of ruby was about 2 cubic centimeters. In contrast, the current design uses only about 0.1 cubic centimeter. Of course the group delay of the current maser can be increased by simply adding more ruby resonators.

The polarization properties of ruby have been discussed previously at length [10]. For completeness, they will be summarized here briefly. This design uses ruby whose c-axis makes an angle of 54.7 deg to the dc biasing magnetic field. The dc field is aligned perpendicular to the broad wall of the waveguide containing ruby; we label this the y-direction. To excite the signal transition, the microwave magnetic field would ideally be circularly polarized in the x–z plane. The fields in the ruby resonators are essentially linearly polarized, due to the large standing wave present. In the TE_{10} waveguide mode, the magnetic field lies entirely in the x–z plane, and it is therefore a suitable and convenient mode to use. A similar
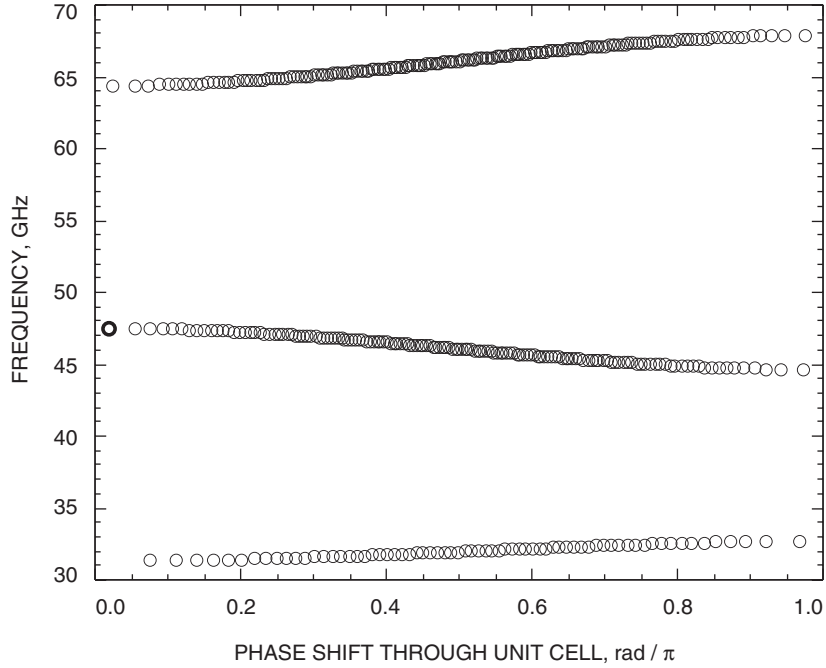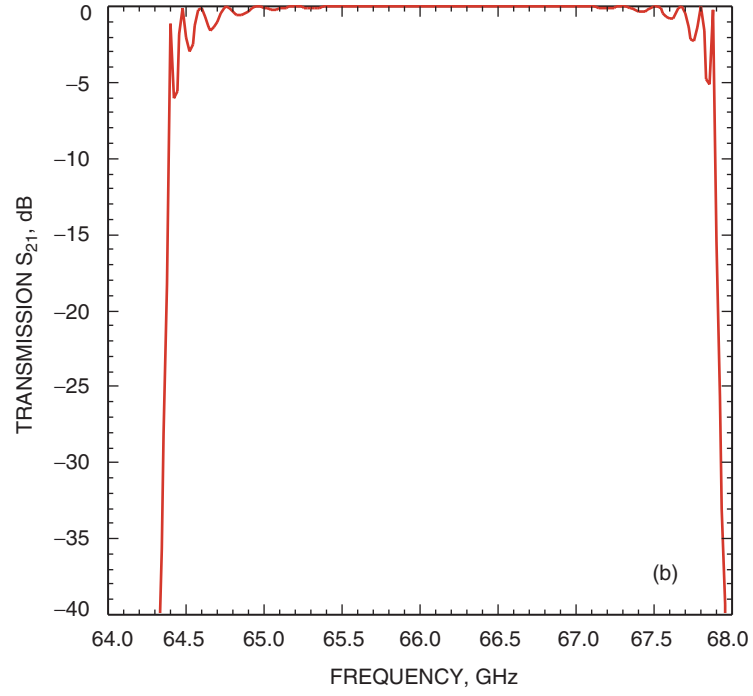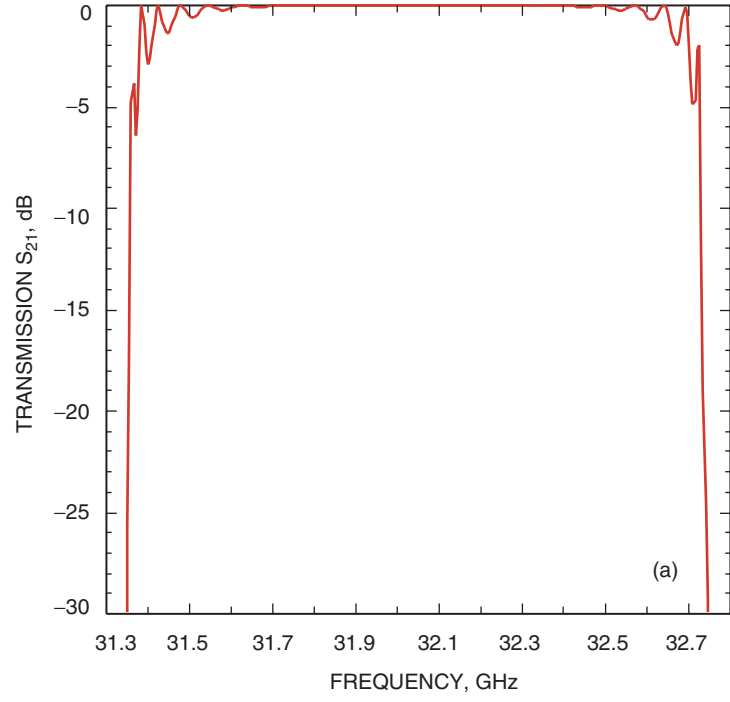

Fig. 3. Frequency versus phase shift for the SWS.

Fig. 4. Calculated transmission response of one arm of the SWS at (a) signal frequencies and (b) pump frequencies.
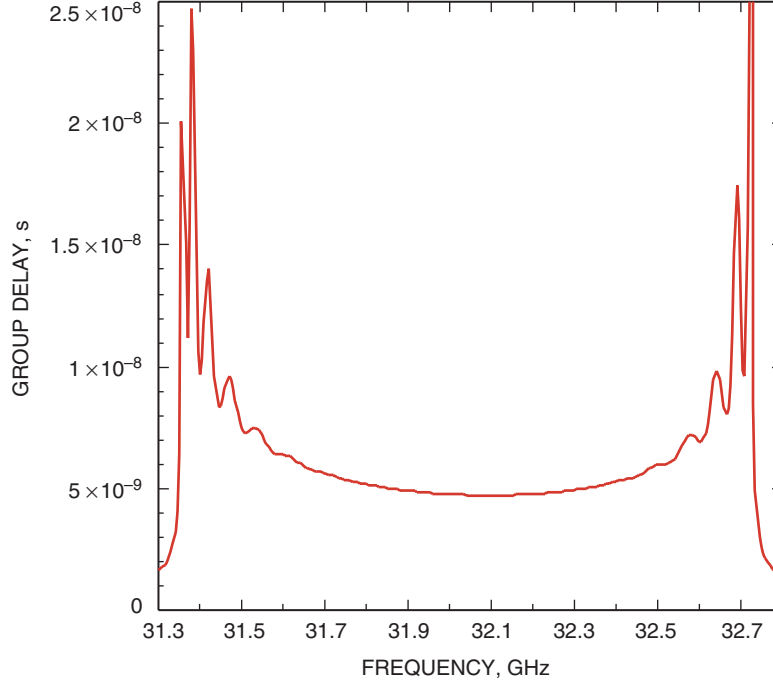
Fig. 5. Calculated group delay of one arm of the SWS.

argument can be made for the pump transitions. In this case, there is some amplitude for a quantum transition for y-directed microwave magnetic fields, but the amplitude is greater in the x- and z-directions. Therefore, the TE$_{10}$ waveguide mode is used also for the pump.

V. Signal Input–Output Circuit

The input–output circuit refers to that portion of Fig. 1(b) between planes a–b and a′–b′. The signal enters the maser in WR-28 rectangular waveguide and then passes through an E-plane mitre bend. After passing through the bend, the air-filled WR-28 is reduced to 0.1740 cm (0.0685 in.)-wide sapphire-filled waveguide using inhomogeneous quarter-wave transformers. In order to simplify the machining, the steps are asymmetric with respect to the waveguide height. For performance reasons, they remain centered in the waveguide width. The dimensions were checked with a mode-matching program. Next an H-plane mitre bend is used to turn the waveguide and align it with the SWS. The right angle turns are used to provide adequate physical separation between the input and output waveguides. Figure 6 shows the calculated input return loss for the input–output circuit.

Quarter-wave transformers are necessary to match the signal traveling in the sapphire-filled waveguide to the much higher impedance of the Bloch wave traveling on the periodic slow-wave structure. These are shown in Fig. 1(b) between planes b–c and b′–c′, and further expanded in Fig. 2. The appendix contains an equation for the Bloch impedance. Knowing both the propagation constant and impedance, quarter-wave matching transformers can be designed in the following way. Each intermediate "step" composing the quarter-wave transformer has the "unit cell" configuration. Knowing the Bloch impedance of the SWS, the required intermediate step impedances are calculated using conventional impedance-matching theory, as discussed in [12]. These impedances correspond to the Bloch impedances of the unit cells forming the intermediate steps. The lengths of the ruby sections and evanescent sections composing each step are adjusted until the required Bloch impedances are obtained and the electrical length of each step is 90 deg. The calculated return loss for one arm of the SWS with impedance-matching transformers on both ends is shown in Fig. 7.
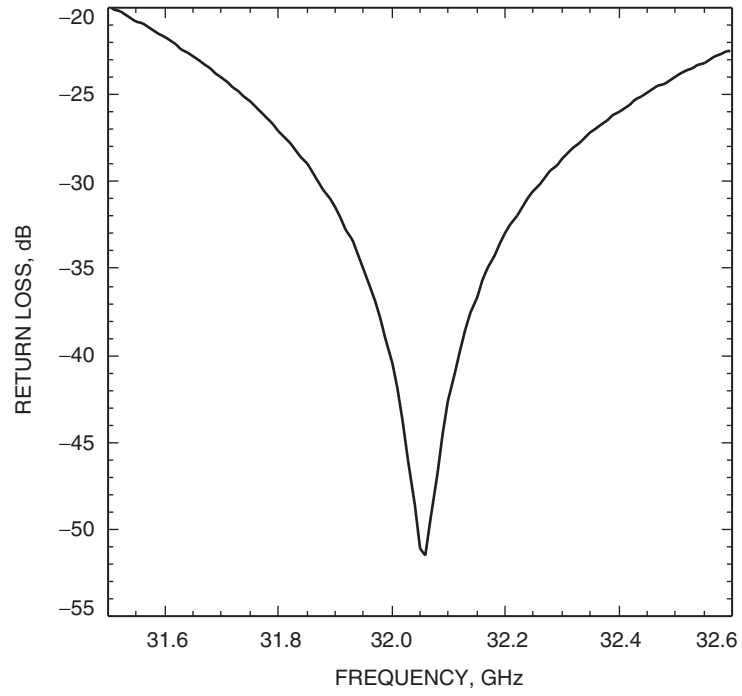
8

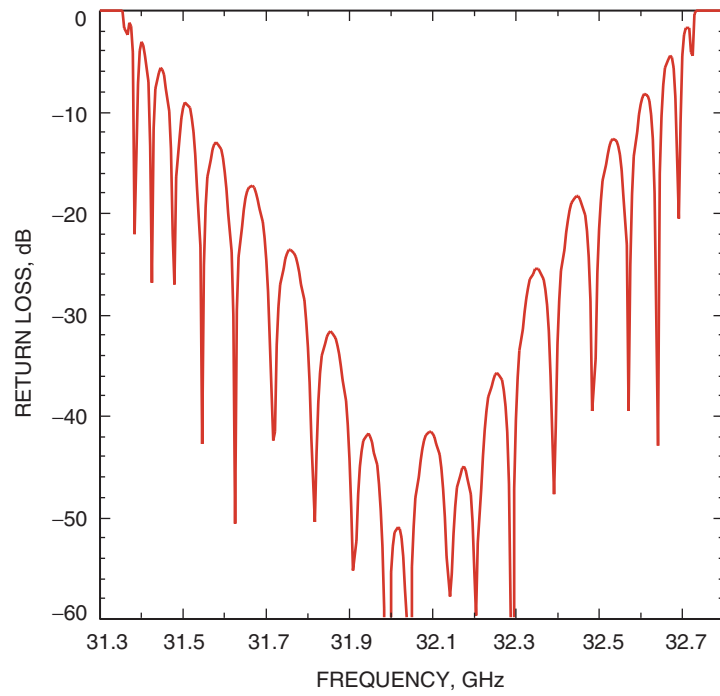**Fig. 6. Calculated return loss of the input circuit.**

Fig. 7. Calculated return loss of one arm of the SWS.

VI. U-Turn Cavity

There are several possible ways to inject the pump energy into the SWS. One approach would be to locate a separate pump waveguide adjacent to the signal waveguide with coupling holes in the side walls between the evanescent sections and the pump waveguide. This idea was rejected because of the anticipated machining difficulties. Another approach is to "break" the SWS in the middle and inject the pump energy there. This is the approach taken.

The cavity is simultaneously resonant at the signal and pump frequencies. The resonant frequency of a closed rectangular cavity of width, height, and length a, b, l is given by [14]

$$f^2 = \frac{c^2}{\varepsilon} \left[\left(\frac{m}{2a} \right)^2 + \left(\frac{n}{2b} \right)^2 + \left(\frac{p}{2l} \right)^2 \right]$$

where c is the speed of light and ε is the relative dielectric constant of the material filling the cavity. Also, m, n, p are the number of half-wavelengths in the width, height, and length of the cavity. For a cavity resonance with no field variation in the height, this equation can be written as

$$a^2 = \frac{c^2}{4f^2\varepsilon} \left\{ m^2 + p^2 \left(\frac{a^2}{l^2} \right) \right\}$$

A plot of a^2 versus a^2/l^2 will yield a straight line whose slope and intercept depend on the mode and the frequency. A cavity filled with a material of relative dielectric constant $\varepsilon = 2.0$ was chosen. Two families of curves, one for $f = 32.05$ GHz and the other for $f = 66.25$ GHz, can be plotted. Where the curves cross, a cavity simultaneously resonant at the signal and pump frequencies exists. Figure 8 shows two lines corresponding to $m = 3$ and $p = 1$ at 32.05 GHz (dashed) and $m = 4$ and $p = 3$ at 66.25 GHz (solid). The point of intersection corresponds to $a = 1.2261$ cm (0.4827 in.) and $l = 0.5613$ cm (0.221 in.). These are the unloaded cavity dimensions. The attachment of input and output waveguides will load the cavity and change the resonant frequencies slightly. The dimensions of the cavity used in the design are 1.2192 cm (0.4800 in.) by 0.5588 cm (0.220 in.) by 0.1016 cm (0.040 in.). Figure 9 shows the calculated insertion loss and return loss of the two arms of the slow-wave structure joined by the U-turn cavity. The presence of the pump injection circuit, to be described next, is also included in the calculation.

VII. Pump Injection Circuit

The pump injection circuit is shown between planes e–e′ and f in Fig. 1. To maintain equal power splitting, a symmetrical structure was chosen. One approach would use a single waveguide entering at the center of the cavity. Another approach uses two waveguides symmetrically located about the centerline. We adopted the latter approach. Two waveguides located near the edges of the cavity are used to couple the pump energy to the cavity. These waveguide ports are properly sized and located so their effect on the signal propagation is minimized.

As mentioned above, the resonant mode for the pump frequency is the TE_{403} mode. This requires the fields in the pump waveguide be phased 180 deg apart. In order to achieve the proper phasing, an E-plane T-junction is used. These junctions have the property that the waves in the output arms are equal in amplitude and opposite in phase. In order to achieve a good input impedance match, a tuning post is symmetrically placed at the base of the T-junction. The post diameter is 0.0762 cm (0.030 in.). The junction is designed with a standard WR-15 waveguide input, and the output arms are 0.3759 cm (0.148 in.) by 0.1016 cm (0.040 in.). Upon leaving the junction, the pump power travels through H-plane mitre bends and is coupled to the cavity feed lines with two impedance-matching quarter-wave transformers. The mitre bends have corners with 0.1588 cm (0.0625 in.) radii to simplify the machining.
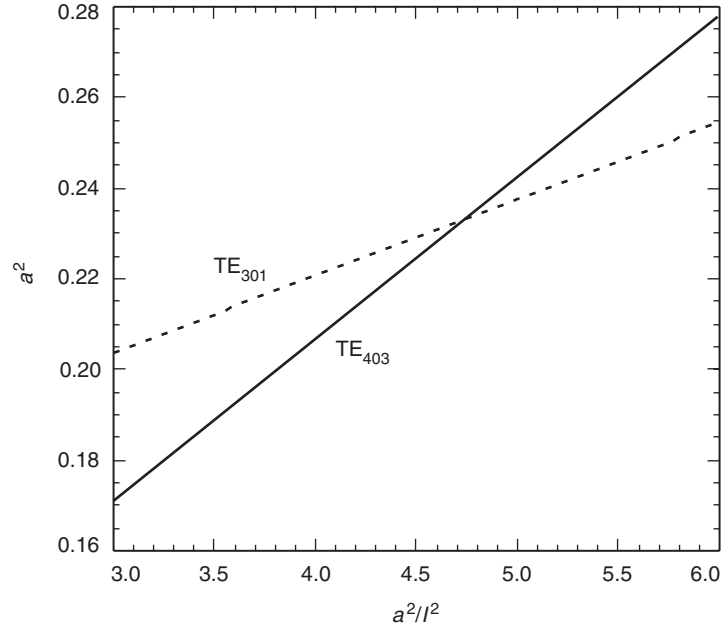
Fig. 8. TE$_{301}$ mode resonance and TE$_{403}$ mode resonance versus cavity dimensions.
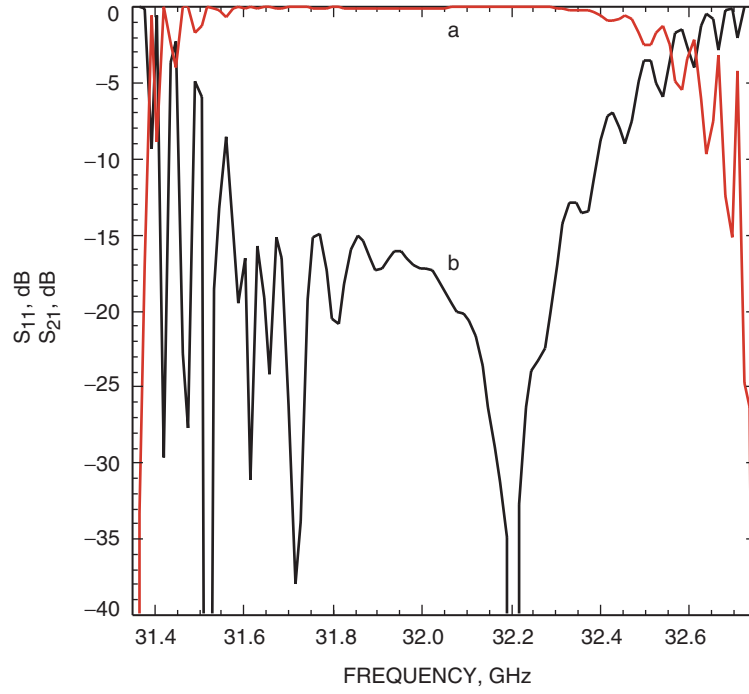

Fig. 9. Calculated forward transmission (curve a) and return loss (curve b) of the microwave structure between planes b–b'.

The pump injection circuit design was evaluated by replacing the portion of the maser between planes a and c and planes a′ and c′ in Fig. 1 with transformers designed to match the SWS at the pump frequencies. The transmission scattering parameter from the pump power input port at plane f to either output port at plane b was calculated. If the pump circuit was functioning ideally, the transmission loss would be 3 dB (half the power goes into each arm) and the input return loss would look well matched. The calculated transmission and reflection scattering parameters are shown in Fig. 10.

VIII. Magnetic Field Profile

In order to broaden the ruby paramagnetic resonance line width, a slightly different dc biasing magnetic field is required over each ruby resonator. A linear field taper is the simplest to build. The linear taper can be applied in any direction. Two choices are along the direction of propagation and perpendicular to it. The latter taper gives a more uniform noise temperature performance, since all frequencies in the pass band are amplified simultaneously. However, the electrical behavior of the SWS is such that the z- and x-components of the microwave magnetic field in the ruby are not equal.

Plots of the magnitude of the z- and x-components of the microwave magnetic field at 32.05 GHz are shown in Figs. 11(a) and 11(b). The z-component is strongest near the side walls, where its value ranges from about 5 to $8.5(\sqrt{\Omega} - \text{in})^{-1}$. It vanishes along the centerline of the SWS. The x-component is strongest at the front and rear faces of the ruby, where its value ranges from zero at the side walls to about $4.5(\sqrt{\Omega} - \text{in})^{-1}$ in the center of the waveguide. It also vanishes at the center of the ruby perpendicular to the direction of propagation. These plots suggest that the best taper is linear along the direction of propagation.

When using such a taper, there will be "gaps" in the biasing field due to the presence of the evanescent sections in the slow-wave structure. These can be compensated for by shifting the linear taper over one arm of the maser structure slightly with respect to the other arm. The frequency shift is chosen so that the resonant frequency in the center of the first ruby in one arm matches that of the resonant frequency in the center of the first evanescent section in the other arm. This shift is accomplished by adding a small
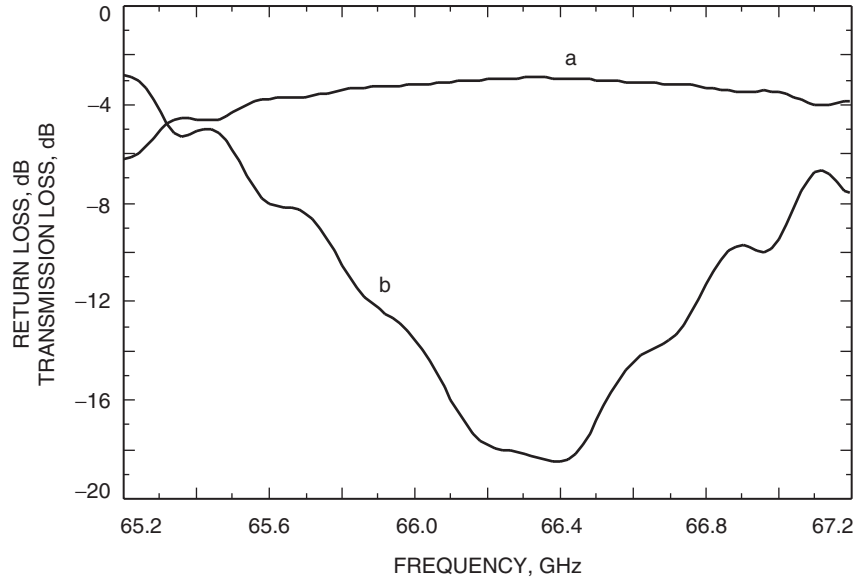

Fig. 10.   Calculated forward transmission (curve a) and return loss (curve b) looking into the pump power injection port at plane f. The two arms of the SWS are terminated at plane c–c' with matched loads at the pump frequencies.

(a)

$|Hz|\ (\sqrt{\Omega}-\text{in})^{-1}$

PROPAGATION
DIRECTION

WAVEGUIDE
WIDTH
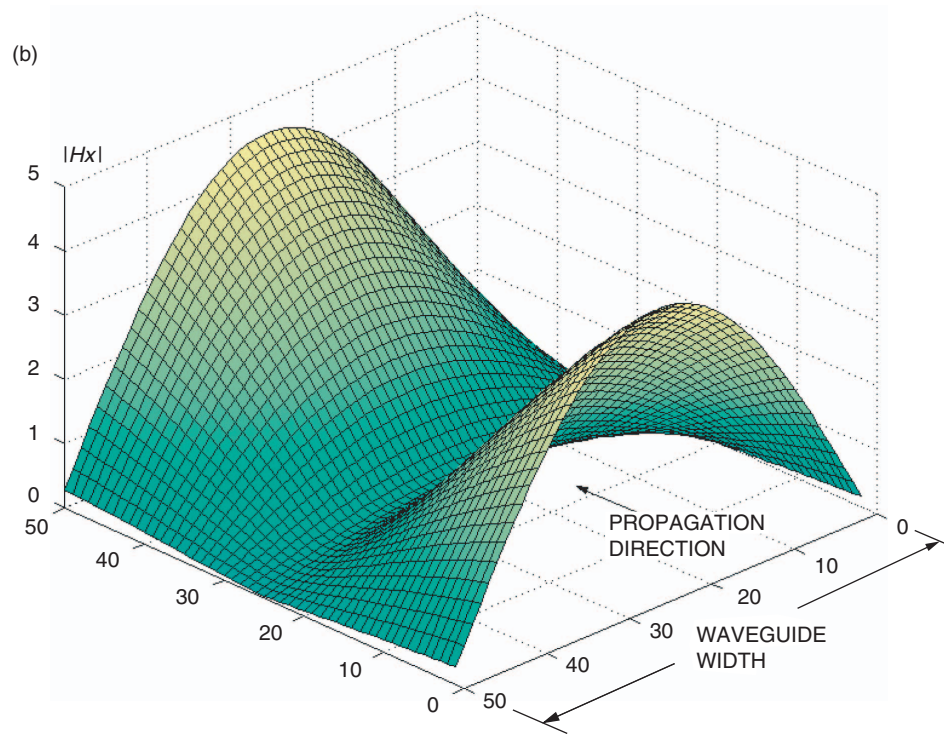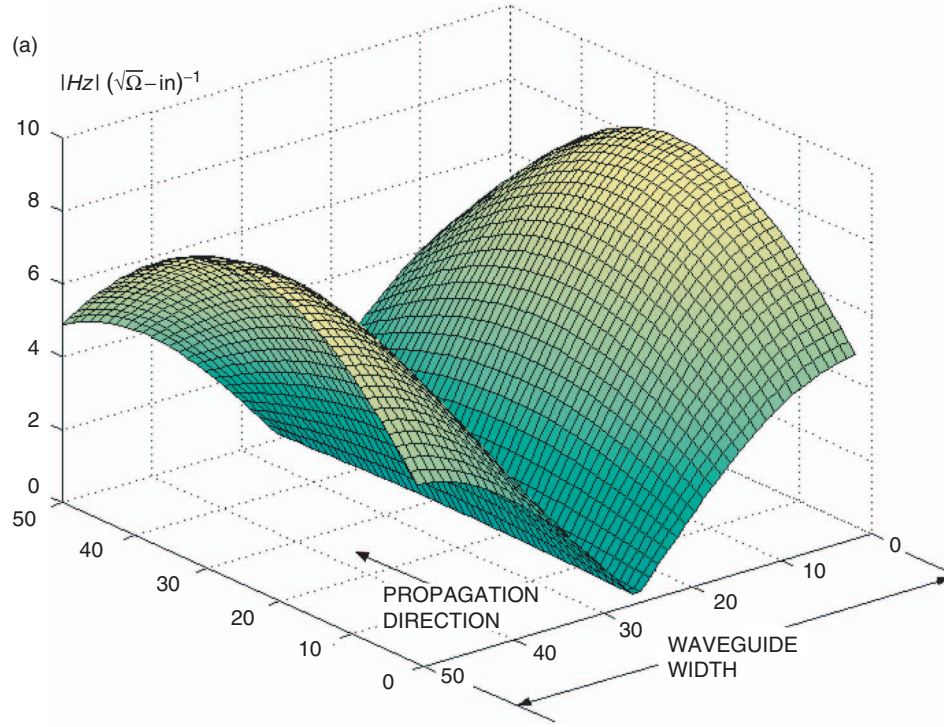
(b)

$|Hx|$

PROPAGATION
DIRECTION

WAVEGUIDE
WIDTH

Fig. 11.   Components of the microwave magnetic field in a ruby section of the SWS at
32.05 GHz: (a) z-component and (b) x-component.

shim to the bias magnet's hiperco pole piece. Now some portion of a ruby is resonating at all frequencies in the pass band. The required field at the input end is 11,778 G, and at the pump end it is 12,005 G. So the field gradient is about 2 percent of the field strength. The required transverse step is about 12 G, or about 0.1 percent of the field strength.

The longer the length of the SWS, the less field gradient there is over any single ruby section, and the smaller the gap in resonant frequency in the evanescent section. The percentage of the taper residing in the gap regions remains the same, but the frequency jump across each gap region becomes a smaller percentage of the 60-MHz natural ruby line width.

The ruby absorption can be calculated with this magnetic field profile using the program mentioned in Section II. For 32 rubies (16 in each arm), the calculated absorption at 4.0 K is shown in Fig. 12. The taper has been adjusted to give nearly the full 500-MHz bandwidth instantaneously. (The calculation does not include dielectric or ferrite losses, only the spin system). Alternatively, one can reduce the magnetic field staggering and achieve greater absorption (and correspondingly greater gain when amplifying) over a narrower instantaneous bandwidth. Figure 13 shows several curves corresponding to a reduced magnetic field taper. This gives increased ruby absorption over a moderate frequency range. The three curves correspond to different average values of the dc magnetic field. These are achieved by changing the current through the superconducting coil.

IX. Resonant Ferrite Isolator

Signal energy traveling in the reverse direction through the slow-wave structure of a TWM must be attenuated. All DSN TWMs use yttrium iron garnet (YIG) resonant isolators for this purpose. The amount of isolation needed to prevent excessive gain ripple exceeds the sum of the forward and reverse direction gain of the TWM. The ruby resonators used in this TWM design provide equal gain in both the forward and the reverse directions. To assure regenerative/degenerative gain ripple of less than 0.2 dB, the isolation should be 40 dB more than twice the TWM net gain in decibels. This isolator characteristic was verified during the development and production of many lower-frequency DSN TWMs. The isolator used in a TWM with 30 dB of net gain must have at least 100-dB reverse loss.
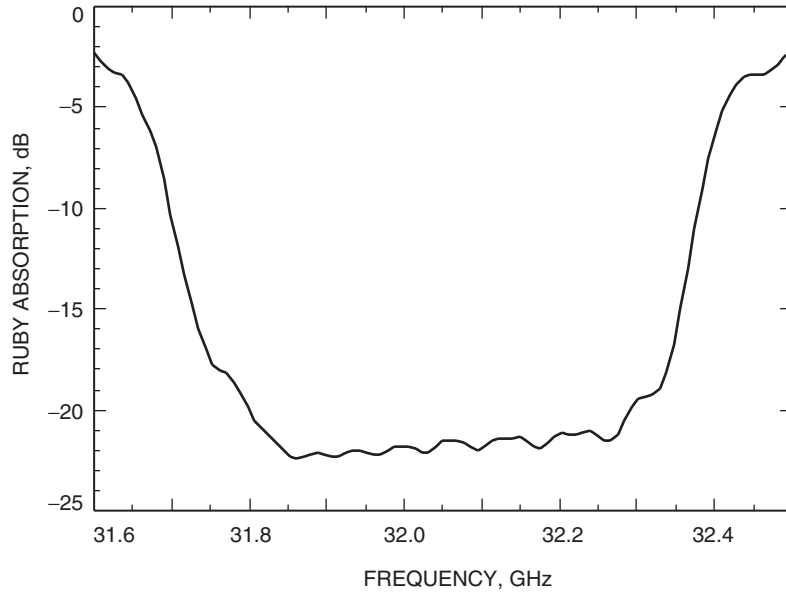

**Fig. 12. Calculated ruby absorption at 4.0 K
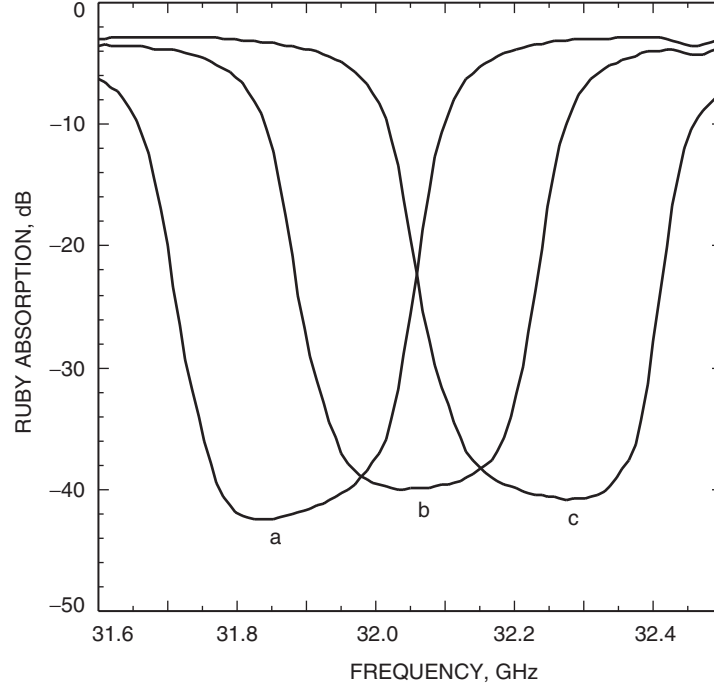(with wide dc magnetic field taper).**

Fig. 13. Calculated ruby absorption at 4.0 K with a magnetic field taper that broadens the ruby linewidth to 350 MHz. Curves a, b, and c correspond to ruby resonance linewidths centered at 31.875 GHz, 32.05 GHz, and 32.225 GHZ, respectively.

Resonance isolators in a TWM are formed using relatively small pieces of ferromagnetic material. Polycrystalline YIG has been used as a resonance isolator material in many TWMs for more than 40 years. YIG pieces are located in regions where the ellipticity of the rf magnetic field polarization approaches one (nearly circular), and where the rotation is of the proper sense. This was explained theoretically and verified experimentally by workers at Bell Labs [15]. The well-defined and quantified regions of circular and elliptical polarization, as analyzed by the computer programs that were developed for this maser design, determine the optimum location for the resonance isolators. Figure 14 shows the microwave magnetic field polarization in the evanescent sections of the SWS. As expected, regions of opposite circular polarization are present.

It is necessary to adjust the shape of the ferrite to achieve ferrite and ruby resonance at the same magnetic field strength. For an ellipsoidal resonator, the resonant frequency is given by [14]

$$(f_o)_{\mathrm{MHz}} = 2.8\sqrt{\big(H_o - (N_z - N_x)(4\pi M_s)\big)\big(H_o - (N_z - N_y)(4\pi M_s)\big)}$$

where N_x, N_y, and N_z are demagnetizing factors in the x-, y-, and z-directions. H_o has units of oersteds, and the saturation magnetization, $4\pi M_s$, of the ferrite has units of gauss. In the above equation for a sphere, $N_x = N_y = N_z = 1/3$. Thus, $f_o = 2.8H_o$, independent of the saturation magnetization. For a right circular cylinder, the demagnetizing factors are not strictly defined, since the magnetization inside the cylinder is not uniform. However, demagnetization factors are still used, and the approximation is made that $N_x = N_y$ if the applied field is along the axis of the cylinder in the z-direction.
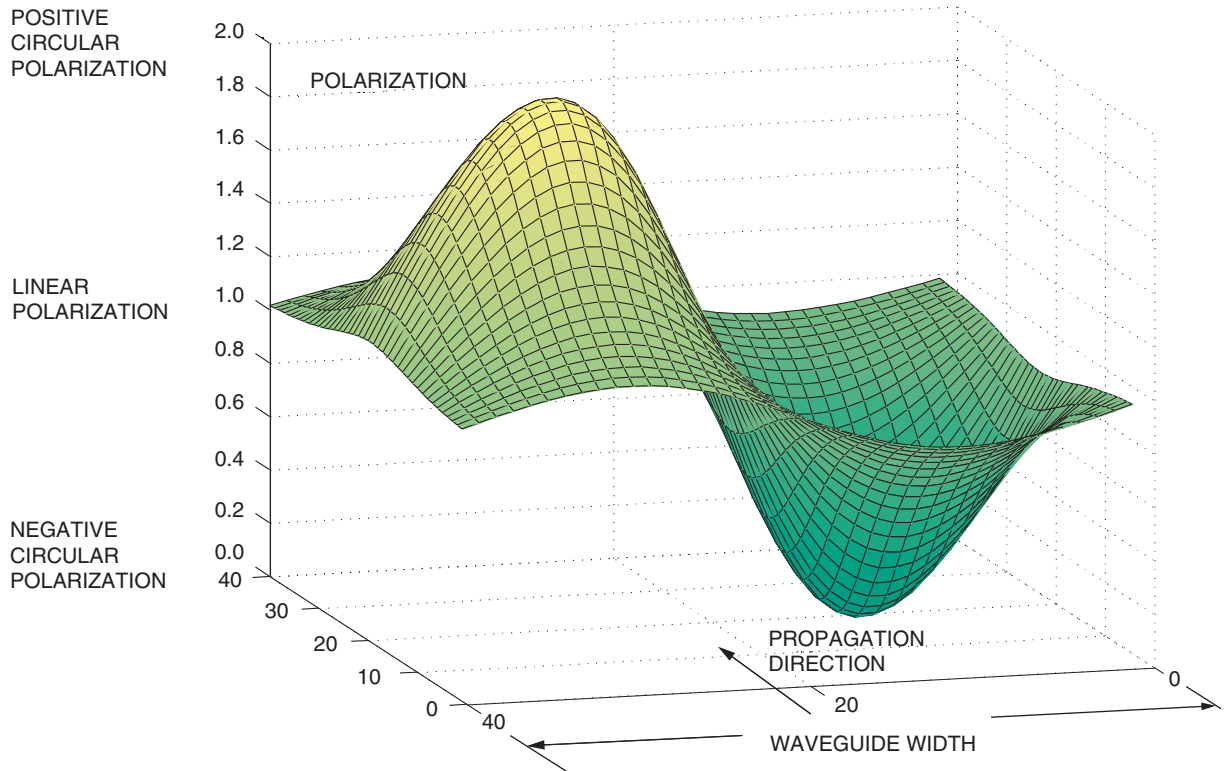
Fig. 14. Microwave magnetic field polarization in the evanescent sections of the SWS.

The dc biasing magnetic field required by the ruby can be found by solving the ruby spin Hamiltonian [10]. A resonance frequency of 32.05 GHz requires a dc magnetic field strength of approximately 11,900 G. At 11,900 G, a ferrite sphere would resonate at 33.32 GHz. Therefore, the spherical shape must be modified to lower the resonant frequency by 1.27 GHz. A slight change of the spherical ferrite shape is planned, by removing a segment of the sphere and providing a flat mounting surface. The amount of material to be removed to achieve the proper resonant frequency will be calculated and verified experimentally. The isolator performance of modified spheres will be compared with the performance of right circular cylinders.

X. Noise Performance Estimate and Discussion

A rigorous calculation of the noise temperature performance of the current maser design cannot be made at this time. It requires a calculation appropriate to a series of coupled half-wavelength transmission cavities with finite isolation between them. Stelzried analyzed the noise behavior of a similar coupled-cavity transmission maser built by the Hughes Research Laboratories [16,17]. His approach was noteworthy in its attempt to deal with the noise power radiated backward from the isolators into the previous gain stages. However, his calculation ascribed all the forward dissipative losses to the isolators and assumed their reverse loss was infinite. In the end, his approach indicates that for net gains of 30 or 40 dB, the calculated performance for 25 coupled cavities only slightly exceeds that of the uniform traveling-wave maser. Since the design presented in this article uses 32 cavities, we will estimate the noise performance using an expression appropriate to a traveling-wave maser. A more rigorous calculation is in preparation. From [18],

$$T_{amp} = \frac{(G-1)}{G} \frac{hf}{k} \left(\frac{G_{el}^{(\text{dB})}}{G_{\text{net}}^{(\text{dB})}} \cdot \frac{r}{r-1} + \frac{L_o^{(\text{dB})}}{G_{\text{net}}^{(\text{dB})}} \cdot \frac{1}{e^{hf/kT_o} - 1} \right)$$

Here L_o is the forward dissipative loss, G_{net} is the net forward gain, and G_{el} is the electronic gain, all expressed in decibels. G is the net gain (not in decibels), h is Planck's constant, k is Boltzmann's constant, and f is the signal frequency. The variable r is related to the spin temperature, T_s, by the equation

$$r = e^{-hf/kTs}$$

and is determined by the inverted spin population. Finally, T_o is the physical temperature of the ruby.

The forward dissipative loss is composed of the ohmic loss in the waveguide, the dielectric losses in the ruby, and the forward loss through the resonant isolator. The dissipative loss for the dominant TE_{10} mode in rectangular waveguide is given by [19]

$$\alpha = \sqrt{\frac{\omega\varepsilon}{2\sigma}} \frac{1}{b} \frac{\left(1 + \frac{2b}{a} \left(\frac{\lambda}{2a} \right)^2 \right)}{\sqrt{1 - \left(\frac{\lambda}{2a} \right)^2}}$$

where a and b are the width and height of the waveguide. Also, $\omega, \varepsilon, \sigma$, and λ are the radian frequency, dielectric constant of the medium filling the guide, conductivity of the metal waveguide walls, and wavelength in the medium filling the guide, respectively. At 32 GHz, a 0.174 cm (0.0685 in.) by 0.102 cm (0.040 in.) waveguide filled with $\varepsilon = 10$ material, and wall conductivity equal to $5.8 \cdot 10^{-7}$ mhos/m, has an attenuation constant of 0.03455 nepers/in., or 0.3 dB/in. The group delay through 50.8 cm (20 in.) of this guide is about 10 ns. Therefore, the estimated room temperature ohmic loss is about 6.0 dB. At 4 K, this ohmic loss should be about 2.0 dB total, or 1.0 dB per arm of the SWS. We will neglect the dielectric losses in the ruby for the purposes of this estimate.

In order to calculate the forward isolator loss, we use the rule of thumb that the total round-trip loss should be twice the electronic gain (in decibels) plus 30 dB. This rule is applied to each separate section of the slow-wave structure. In the present design, this rule would apply to the portions of the SWS before and after the U-turn cavity. In wide-bandwidth operation, the ruby absorption has been calculated to be about 22 dB, or 11 dB for each arm of the SWS. Assuming an inversion ratio of 1.3, the electronic gain of each arm will be 14.3 dB. Twice the round-trip gain plus 30 is 58.6 dB. Subtracting the forward and reverse ohmic loss (2.0 dB) leaves 56.6 dB for the round-trip isolator loss. Assuming the isolator front-to-back ratio is 1:30, the forward isolator loss will be about 1.83 dB per arm. Therefore, the total forward dissipative loss of the complete maser is 5.7 dB. This is the value we use for L_o. Assuming a physical temperature of 4.0 K, $G_{el} = 28.6$ dB, and $G_{\text{net}} = 22.9$ dB, the maser noise temperature is estimated to be 6.0 K at the cryogenic input.

Similarly, for moderate-bandwidth operation, the ruby absorption is calculated to be 40 dB, or 20 dB per arm. The corresponding electronic gain per arm is 26 dB. The required round-trip loss is 82 dB. Subtracting 2.0 dB for the round-trip ohmic loss leaves 80 dB for the total forward and reverse isolator loss. Again assuming a front-to-back ratio of 1:30 implies 2.58 dB of forward isolator loss per arm. The total forward dissipative loss for the complete maser is 7.2 dB, and the net gain is 44.8 dB. With a bath temperature of 4.0 K, the maser noise temperature is estimated to be 5.3 K at the cryogenic input. In both cases, the quantum noise is included.

Before the maser design presented in this article can be finalized, a number of parameters must be determined experimentally. The anisotropic dielectric constant of sapphire at room temperature is reasonably well known [20]. An effective dielectric constant, when the microwave electric field is not along a principal axis of the dielectric tensor, can be estimated using an expression from Goodwin et al. [21]. They give the effective dielectric constant for ruby as

$$\frac{1}{\varepsilon_{eff}} = \frac{\cos^2\theta}{\varepsilon_{||}} + \frac{\sin^2\theta}{\varepsilon_\perp}$$

where θ is the angle between the microwave electric field vector and the ruby optic axis. In the present case, the microwave electric field is aligned along the dc magnetic field. It makes an angle of 54.7 deg with the optic axis. Using $\varepsilon_{||} = 11.49$ and $\varepsilon_\perp = 9.34$ yields an effective dielectric constant of 10.0. The current design used a value 1 percent larger than this. The dielectric constant may change upon cooling to a 4-K physical temperature. Therefore, a test slow-wave structure with samples of the ruby to be used will be built and cooled to determine the effective dielectric constant at cryogenic temperatures.

Another concern is the presence of small air gaps above the rubies. These air gaps modify the wave impedance and electrical length. This problem is currently under theoretical investigation. There may be situations where the change can be employed to help realize some of the quarter-wave transformers.

The maser design depends on the physical operating temperature. This is determined by the thermal loading of the cooler (including pump power) and the desired cooling capacity margin. The ruby inversion ratio depends on the physical operating temperature, the pumping efficiency, and the relaxation times between levels. It is likely to be in the range of 1.0 to 1.5 [22]. This affects the gain of the maser. The gain determines the required amount of ferrite isolator material. Although the proper location of the ferrite has been indicated in this article, the size and shape of the ferrite remain to be investigated.

A Ka-band traveling-wave maser design has been presented. A key feature is a slow-wave structure composed of alternating sections of ruby-filled and evanescent waveguide. This gives high slowing factors at both the signal and pump frequency bands. This leads to a large gain–bandwidth product at signal frequencies and good pumping efficiency. This maser design is intended for operation in 4-K closed-cycle G-M refrigerators. An additional cooling loop can be added for below 4-K operation [23], which would result in higher performance. Its application is primarily for the 34-m and larger antennas in the Deep Space Network.

Acknowledgment

References

[1] J. S. Shell and R. C. Clauss, "A 32-GHz Coupled-Cavity Maser Design," *The Telecommunications and Mission Operations Progress Report 42-142, April–June 2000*, Jet Propulsion Laboratory, Pasadena, California, pp. 1–22, August 15, 2000. http://tmo.jpl.nasa.gov/tmo/progress_report/42-142/142G.pdf

[2] W. H. Higa and E. Wiebe, "A Simplified Approach to Heat Exchanger Construction for Cryogenic Refrigerators," *Cryogenic Technology*, vol. 3, pp. 47–51, March/April 1967.

[3] T. R. Hanson, "Helium Compressors for Closed-Cycle, 4.5-Kelvin Refrigerators," *The Telecommunications and Data Acquisition Progress Report 42-111, July–September 1992*, Jet Propulsion Laboratory, Pasadena, California, pp. 246–253, November 15, 1992.
http://tmo.jpl.nasa.gov/tmo/progress_report/42-111/111U.PDF

[4] D. L. Johnson, S. M. Petty, J. J. Kovatch, and G. W. Glass, "Ultralow Noise Performance of an 8.4-GHz Maser–Feedhorn System," *The Telecommunications and Data Acquisition Progress Report 42-100, October–December 1989*, Jet Propulsion Laboratory, Pasadena, California, pp. 100–110, February 15, 1990.
http://tmo.jpl.nasa.gov/tmo/progress_report/42-100/100I.PDF

[5] J. Shell and R. B. Quinn, "A Dual-Cavity Ruby Maser for the Ka-Band Link Experiment," *The Telecommunications and Data Acquisition Progress Report 42-116, October–December 1993*, Jet Propulsion Laboratory, Pasadena, California, pp. 53–70, February 15, 1994.
http://tmo.jpl.nasa.gov/tmo/progress_report/42-116/116f.pdf

[6] J. Shell, "Radio Frequency Fields in Multiple-Cavity Masers," *The InterPlanetary Network Progress Report 42-146, April–June 2001*, Jet Propulsion Laboratory, Pasadena, California, pp. 1–14, August 15, 2001.
http://ipnpr.jpl.nasa.gov/tmo/progress_report/42-146/146H.pdf

[7] J. Shell, "A Spin System Model for Coupled-Cavity Masers," *The Interplanetary Network Progress Report 42-151, July–September 2002*, Jet Propulsion Laboratory, Pasadena, California, pp. 1–16, November 15, 2002.
http://ipnpr.jpl.nasa.gov/tmo/progress_report/42-151/151C.pdf

[8] D. J. Hoppe, "Modal Analysis Applied to Circular, Rectangular, and Coaxial Waveguides," *The Telecommunications and Data Acquisition Progress Report 42-95, July–September 1988*, Jet Propulsion Laboratory, Pasadena, California, pp. 89–96, November 15, 1988.
http://tmo.jpl.nasa.gov/tmo/progress_report/42-95/95I.PDF

[9] MATLAB, Version 5, The MathWorks, Inc., Natick, Massachusetts, Copyright 1984–1998.

[10] J. Shell, "The Paramagnetic Ground State of Ruby—Revisited," *The Interplanetary Network Progress Report 42-150, April–June 2002*, Jet Propulsion Laboratory, Pasadena, California, pp. 1–14, August 15, 2002.
http://ipnpr.jpl.nasa.gov/tmo/progress_report/42-150/150K.pdf

[11] WASP-NET, Waveguide Synthesis Program for Waveguide Networks, Microwave Innovation Group, Bremen, Germany.

[12] R. E. Collin, *Foundations for Microwave Engineering*, New York: McGraw-Hill Book Company, 1966.

[13] J. Shell and D. Neff, "A 32-GHz Reflected-Wave Maser Amplifier With Wide Instantaneous Bandwidth," *The Telecommunications and Data Acquisition Progress Report 42-94, April–June 1988*, Jet Propulsion Laboratory, Pasadena, California, pp. 145–162, August 15, 1988.
http://tmo.jpl.nasa.gov/tmo/progress_report/42-94/94L.PDF

[14] G. Matthei, L. Young, and E. M. T. Jones, *Microwave Filters, Impedance Matching Networks, and Coupling Structures*, Norwood, Massachusetts: Artech House, 1980.

[15] F. S. Chen and W. J. Tabor, "Filling Factor and Isolator Performance of the Traveling-Wave Maser," *The Bell System Technical Journal*, vol. 43, pp. 1005–1033, May 1964.

[16] C. T. Stelzried, "XV. Communications Elements Research, A. Low-Noise Amplifiers," *JPL Space Programs Summary 37-23*, Jet Propulsion Laboratory, Pasadena, California, pp. 203–212, 1963.

[17] F. E. Goodwin, J. E. Kiefer, and G. E. Moss, "The Coupled-Cavity Transmission Maser-Engineering Design," *IEEE Transactions on Microwave Theory and Techniques*, MTT-12, pp. 349–358, May 1964.

[18] J. S. Shell, R. C. Clauss, S. M. Petty, G. W. Glass, M. S. Fiore, J. J. Kovatch, J. R. Loreman, D. E. Neff, R. B. Quinn, and D. L. Trowbridge, "Ruby Masers for Maximum G/T_{op}," *Proceedings of the IEEE*, vol. 82, no. 5, pp. 796–810, May 1994.

[19] C. G. Montgomery, R. H. Dicke, and E. M. Purcell, *Principles of Microwave Circuits*, London: Peter Peregrinus Ltd., 1987.

[20] P. H. Ladbrooke, M. H. N. Potok, and E. H. England, "Coupling Errors in Cavity-Resonance Measurements on MIC Dielectrics," *IEEE Transactions on Microwave Theory and Techniques*, vol. MTT-21, p. 560, August 1973.

[21] F. E. Goodwin, J. E. Kiefer, and G. E. Moss, "The Coupled-Cavity Transmission Maser-Engineering Design," *IEEE Transactions on Microwave Theory and Techniques*, vol. MTT-12, pp. 349–358, May 1964.

[22] J. R. Lyons, "Spin-Lattice Relaxation and the Calculation of Gain, Pump Power, and Noise Temperature in Ruby," *The Telecommunications and Data Acquisition Progress Report 42-98, April–June 1989*, Jet Propulsion Laboratory, Pasadena, California, pp. 63–85, August 15, 1989.
http://tmo.jpl.nasa.gov/tmo/progress_report/42-98/98D.PDF

[23] M. Britcliffe, T. Hanson, and J. Fernandez, "A 2.5-Kelvin Gifford–McMahon/ Joule–Thomson Cooler for Cavity Maser Applications," *The InterPlanetary Network Progress Report 42-147, July–September 2001*, Jet Propulsion Laboratory, Pasadena, California, pp. 1–9, November 15, 2001.
http://ipnpr.jpl.nasa.gov/tmo/progress_report/42-147/147F.pdf

Appendix

Propagation Constant and Bloch Impedance of the SWS

The component wave amplitude transmission matrices for the unit cell are given by

$$A_1 = \begin{bmatrix} e^{j\beta l_1} & 0 \\ 0 & e^{-j\beta l_1} \end{bmatrix}$$

$$A_2 = \frac{1}{2\sqrt{z_1 z_2}} \begin{bmatrix} z_1 + z_2 & z_2 - z_1 \\ z_2 - z_1 & z_1 + z_2 \end{bmatrix}$$

$$A_3 = \begin{bmatrix} e^{\kappa l_2} & 0 \\ 0 & e^{-\kappa l_2} \end{bmatrix}$$

$$A_4 = \frac{1}{2\sqrt{z_1 z_2}} \begin{bmatrix} z_1 + z_2 & z_1 - z_2 \\ z_1 - z_2 & z_1 + z_2 \end{bmatrix}$$

$$A_5 = \begin{bmatrix} e^{j\beta l_1} & 0 \\ 0 & e^{-j\beta l_1} \end{bmatrix}$$

where z_1 and z_2 are the impedances of the ruby-filled and evanescent waveguides, respectively. The complete transmission matrix is given by multiplying the above matrices:

$$A = A_1 A_2 A_3 A_4 A_5 =$$

$$\frac{1}{4z_1 z_2} \begin{bmatrix} e^{2j\beta l_1} e^{\kappa l_2}(z_1 + z_2)^2 - e^{2j\beta l_1} e^{-\kappa l_2}(z_2 - z_1)^2 & e^{\kappa l_2}(z_1^2 - z_2^2) + e^{-\kappa l_2}(z_2^2 - z_1^2) \\ e^{\kappa l_2}(z_2^2 - z_1^2) + e^{-\kappa l_2}(z_1^2 - z_2^2) & e^{-2j\beta l_1} e^{-\kappa l_2}(z_1 + z_2)^2 - e^{-2j\beta l_1} e^{\kappa l_2}(z_2 - z_1)^2 \end{bmatrix}$$

If the wave amplitude transmission matrix is denoted by

$$A = \begin{bmatrix} A_{11} & A_{12} \\ A_{21} & A_{22} \end{bmatrix}$$

then according to the theory of periodic structures, the propagation constant of the Bloch wave is given by

$$\cosh(\gamma d) = \frac{A_{11} + A_{22}}{2}$$

where d is the length of the unit cell and γ is the propagation constant. When the right-hand side is less than or equal to one, we must have $\gamma = j\zeta$.

At these frequencies, using $\cosh(j\zeta) = \cos(\zeta)$, we can write

$$\zeta = \frac{1}{2l_1 + l_2} \left(\cos^{-1} \left[\frac{A_{11} + A_{22}}{2} \right] \right)$$

Using the elements of the matrix given above,

$$\frac{A_{11} + A_{22}}{2} = \cos(2\beta l_1)\cosh(\kappa l_2) + \frac{(Z_R^2 - Z_E^2)}{2Z_R Z_E} \sin(2\beta l_1)\sinh(\kappa l_2)$$

where

$$\beta = \sqrt{\left(\frac{2\pi}{\lambda_o}\right)^2 \varepsilon_r - \left(\frac{\pi}{a}\right)^2}, \quad Z_R = \frac{377.6/\sqrt{\varepsilon_r}}{\sqrt{1 - \left(\frac{\lambda}{\lambda_c}\right)^2}}$$

and

$$\kappa = \sqrt{\left(\frac{\pi}{a}\right)^2 - \left(\frac{2\pi}{\lambda_o}\right)^2 \varepsilon_e}, \quad Z_E = \frac{377.6/\sqrt{\varepsilon_e}}{\sqrt{\left(\frac{\lambda}{\lambda_c}\right)^2 - 1}}$$

where ε_r and ε_e are the relative dielectric constants in the ruby and evanescent sections, respectively, and λ and λ_o are the wavelength in the medium filling the guide and the free space wavelength, respectively.

The solution for a Bloch wave requires that

$$\begin{bmatrix} A_{11} & A_{12} \\ A_{21} & A_{22} \end{bmatrix} \begin{bmatrix} c_{n+1}^+ \\ c_{n+1}^- \end{bmatrix} = \begin{bmatrix} c_n^+ \\ c_n^- \end{bmatrix} = e^{-\gamma d} \begin{bmatrix} c_{n+1}^+ \\ c_{n+1}^- \end{bmatrix}$$

where c_n^+ and c_n^- represent the amplitudes of waves propagating in the forward and backward directions, respectively. The Bloch impedance is given by

$$\overline{Z}_B = \frac{1 + \Gamma_B}{1 - \Gamma_B}$$

where

$$\Gamma_B = \frac{c_n^-}{c_n^+}$$

This yields the normalized Bloch impedance in terms of the wave amplitude transmission matrix elements as

$$\overline{Z}_B^{\pm} = \frac{2A_{12} + (A_{22} - A_{11}) \pm \sqrt{(A_{11} + A_{22})^2 - 4}}{2A_{12} - (A_{22} - A_{11}) \mp \sqrt{(A_{11} + A_{22})^2 - 4}}$$

where the normalization is with respect to the sapphire-filled waveguide impedance.